Applied Physics A (2023) 129:827
https://doi.org/10.1007/s00339-023-07118-7

Applied Physics A
Materials Science & Processing

On the memory-switching property of ternary CuZnS thin films

Aabel Premnath[1] · Sai Guru Srinivasan Sathyiyanarayanan[1] · Amiruddin Rafiuddin[2] · Santhosh Kumar Maniyeri Chandroth[1]

Received: 26 June 2023 / Accepted: 29 October 2023 / Published online: 7 November 2023
© The Author(s), under exclusive licence to Springer-Verlag GmbH, DE part of Springer Nature 2023

Abstract

Copper–zinc sulfide (CZS) is a ternary earth-abundant and non-toxic material having a wide range of optoelectronic applications. This investigation presents the bipolar-switching characteristics of CZS-switching layer-based devices for resistive memory-switching applications. The material was deposited on the fluorine doped tin oxide (FTO) substrate by spray pyrolysis method at a substrate temperature of 350 °C. Structural analysis indicate that the as prepared films consists of a composite structure of CuS and ZnS phases. The deposited films are p-type in nature. Resistive memory-switching devices are fabricated with the structure of FTO/CZS/Ag. The observed ON/OFF ratio of ~ 320 suggests that the device possesses good memory-switching properties. The formation and rupture of the conductive filaments of the FTO/CZS/Ag memory device were detected from the hysteresis curve. This confirms that CZS material can be used as the switching layer to fabricate a simple, cost-effective, and non-toxic bipolar device, which can deliver the perfect switching characteristics.

Keywords CZS · Spray pyrolysis · Heterojunction · Bipolar-resistive memristor

1 Introduction

Copper zinc sulphide (CZS) is a ternary material that is reported to have pioneering applications, which include energy production, optoelectronic devices, etc. This material is also found in applications, such as memory-switching devices, which is an emerging area of research. Presently, there are varieties of compounds used for resistive random access memory (RRAM) applications, which include binary metal oxides, such as copper oxide (Cu_xO), zinc oxide (ZnO), nickel oxide (NiO), tungsten oxide (WO_3) etc. [1, 2]. However, the report on the memory-switching devices using sulfide compounds are minimal [3–5]. Implementation of high storage capacity and density, faster writing and reading, and the low energy consumption are some of the major challenges[6]. One or more of the following mechanisms, including the development of the conduction mechanism, the generation of the conductive filament, and dynamic temperature change, can be used to explain resistive switching [7]. The space-charge-limited conduction mechanism (SCLC), trap-assisted tunnelling, and hopping conduction are only a few of the numerous modes that constitute the conduction mechanisms in RRAM devices.

Photovoltaic properties of CZS compound were investigated by Sreejith et al., and Kitagawa et al. [8, 9]. The tuneable band-gap nature and photovoltaic properties of CZS compound were also studied in depth [10, 11]. Due to its high electrical conductivity and agglomerated morphology, the application of CZS in the field of memory switching is promising. Bera et.al. reported the resistive-switching characteristics of a single Zn-doped CuS nanoball [12]. Other chalcogenide-based compounds such as copper–zinc–tin sulphide (CZTS), copper–iron–tin sulphide (CFTS), copper–indium sulphide ($CuInS_2$), etc. are effectively used as active layer materials in memory-switching applications [13–16]. However, the endurance characteristics are rather poor for these compounds.

In the present work, we report the study on the fabrication of RRAM devices, showing electrical bistability using low cost and earth abundant ternary CZS material. Spray pyrolysis method is used for the deposition of CZS films. Memory-switching devices with a structure of FTO/CZS/Ag, with CZS serving as the active layer and FTO serving as the base contact layer are fabricated. The bi-polar-switching character of the

✉ Santhosh Kumar Maniyeri Chandroth
santhoshmc@nitt.edu

[1] Optoelectronic Materials and Devices Laboratory, Department of Physics, National Institute of Technology, Tiruchirappalli, Tamil Nadu 620015, India

[2] Department of Physics, B.S. Abdur Rahman Crescent Institute of Science and Technology, Chennai 600048, India

fabricated devices are investigated by current–voltage (I–V) measurements and reported.

2 Experiment

In this study, chemical spray pyrolysis process is used to deposit CZS thin films.100 ml solution was prepared by dissolving 0.02 molar (M) cupric chloride ($CuCl_2$:$2H_2O$ > 98.5%, Merck), 0.02 molar (M) zinc chloride ($ZnCl_2$ > 95%, Merck), and 0.06 molar (M) thiourea ($(NH_4)_2CS$ > 99%, Merck) in double-distilled water. Fluorine doped tin oxide (FTO) films with sheet resistivity of ~ 8 Ω/sq.cm from sigma Aldrich was used for the back contact. FTO substrates were cleaned with soap solution first and with iso propyl alcohol (IPA) and dried in oven at 80 ℃ for 30 min. The cleaned substrate was placed inside the spray chamber on a heater, where the temperature variations can be monitored, and the solution was sprayed onto it. To achieve a consistent solution spray rate, airflow for spray has been carefully regulated at an ideal value of 0.2 Pa. The precursor flows at a constant rate of 5 ml per minute. The optimization and characterisation of the CZS films with a thickness of ~ 770 nm on soda lime glass substrates at 350 ℃ was reported elsewhere [11]. A thin layer (~ 400 nm) of silver (Ag) contact with an area of 1 mm^2 was deposited on top of the CZS active layer by means of thermal evaporation using a dot-like mask, and it was heated at 70 °C in an oven for 45 min. The final device structure is FTO/CZS/Ag with CZS serving as the active layer. The total area of the device is 32 × 22 mm. Structural studies of CZS thin films deposited at 350 ℃ was carried out using grazing incidence X-ray diffraction (RIGAKU Ultima X-Ray Diffractometer using CuKα energy source of wavelength λ = 1.5406 Å). Raman measurement was carried out using Horiba Lab-RAM HR Evolution Raman Spectrometer using 532 nm Nd-YAG laser with power of 3 mW. Surface morphology of the films was observed from high-resolution field emission scanning electron microscope (FESEM, ZEISS Ultra 55). Energy dispersive spectroscopy (EDS, Oxford) was used to identify the elemental composition of the sprayed CZS thin films. Detailed surface topography and roughness analysis of the sprayed films were carried out using atomic force microscopy (AFM, Park-NX10). Electrical properties were investigated using Ecopia HMS-5000 hall measurement system. I–V measurements and electrical bi-stability have been studied with the help of Keysight-B2901A source measure unit (SMU).

3 Results and discussion

3.1 Structural studies

The X-ray diffraction pattern of the CZS thin films deposited at substrate temperature of 350 °C is shown in Fig. 1. It is observed that the major peak at 2θ value of 28.83° along (111) plane is associated with the rhombohedral ZnS phase. Another small peak at 46.53° corresponds to ZnS phase which is along (116) plane. Both the peaks correspond to the ICDD reference 89–7386. The peak with an ICDD reference of 75–2236 and a 2θ value of 47.86° along the (220) plane is related to the hexagonal CuS phase [10, 17]. In addition to this, the peak at 2θ value of 25.85° corresponds to the ZnS phase with orientation along (101) plane. For the ternary structure of CZS material, neither a conventional structural pattern nor an ICDD reference index have been documented thus far. CZS has been described in a variety of forms, including Cu alloyed ZnS [17], CuS–ZnS binary composite [18], $Cu_xZn_yS_z$ non-stoichiometric alloy form [19], and Zn doped CuS [12]. It is clear from the X-ray diffraction patterns that the structure of the as-deposited films can be assigned to a composite of CuS and ZnS binary phases [13].

The structure of the CZS thin films are further evaluated using Raman studies. Figure 2 shows the Raman spectra of the as-prepared samples. The high intense peak observed at 475 cm^{-1} matches with the standard Cu–S vibration, which corresponds to longitudinal optic (LO) mode. Adding to this, Raman peaks having less intensity is also observed at 263 cm^{-1} and 924 cm^{-1} which resembles the Cu–S–Zn bond vibrations in the LO mode and transverse optic (TO) mode of Cu–S bond vibrations, respectively [10, 11].

3.2 Morphological studies

Figure 3a, b, c shows the FESEM with EDAX and AFM 3D image for the CZS sample deposited at a substrate temperature of 350 ℃ on soda lime glass substrate. Uniform

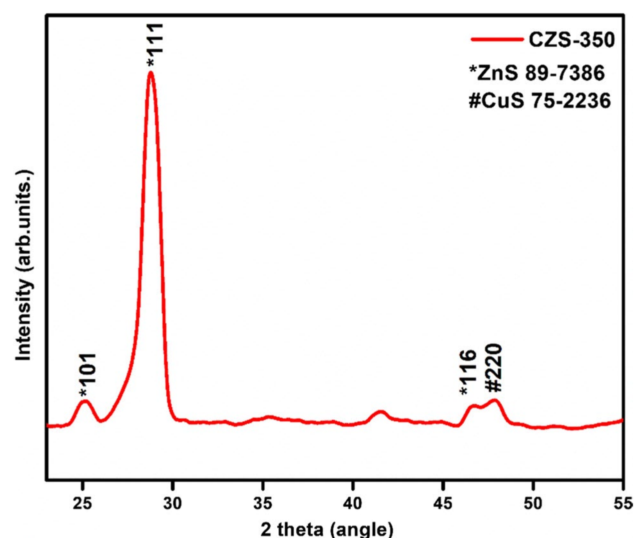

Fig. 1 X-ray diffractogram of the spray deposited CZS film at 350 ℃

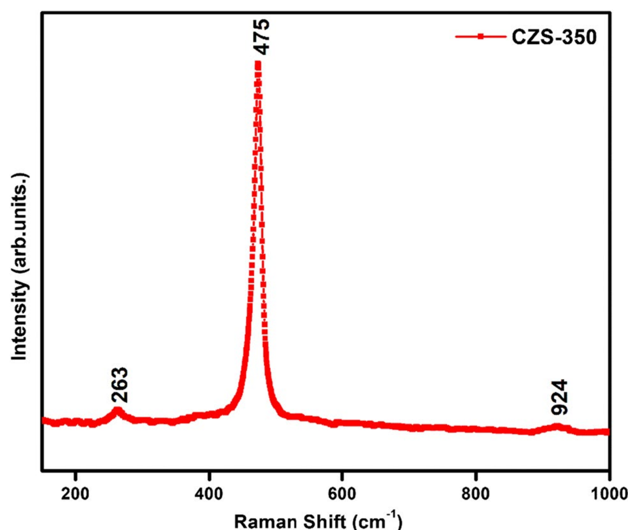

Fig. 2 Raman spectra of the as-deposited CZS thin films at 350 ℃

morphology has been observed for the samples with nano-popcorn-like grain distribution having small flake-like designs. The EDAX spectrum indicate the presence of the elements Cu, Zn and S along with the peaks correspond to Si from the glass substrate. The AFM 3D topography (Fig. 3c) indicates that the particles are agglomerated on the surface of the films. Surface contains dense and agglomerated morphology and the rms roughness value vary from 14.7 to 597 nm for the deposited samples. The depth variation is due to the agglomerated morphology of the deposited thin films. The value of Rq and Ra is observed as 78.6 and 56.6 nm, respectively. Table 1 shows the atomic concentration of constituent elements in the as-prepared CZS samples. The atomic percentage obtained using EDAX measurement is in agreement with the previous report for CZS thin films [11].

3.3 Electrical properties

Hall measurement system is used to study the electrical properties of the as-deposited CZS thin films deposited at 350 °C. The bulk carrier concentration, conductivity and mobility obtained from the measurements are 5.47×10^{19} cm^{-3}, 4.68×10^{2} S cm^{-1} and 53.3 $cm^{2}V^{-1}S^{-1,}$ respectively. The hall measurements also confirmed that the as-deposited films are p-type in nature.

3.4 Resistive-switching characteristics

Hysteresis loop is the defining feature of memristor devices. Figure 4 illustrates the schematic diagram of the fabricated memory device and along with a photograph of the fabricated device. Figure 5a, b shows the log (|I|) – V characteristics of the device in positive and negative bias regions and pinched hysteresis current–voltage (I–V) loops of the FTO/CZS/Ag-resistive-switching device. The delta-V step voltage has been applied in the range from -2 to 2 V and the device exhibits resistive-switching properties by sweeping – 1.45 V to + 0.6 V without the forming voltage.

The switching loop area in CZS-based memory devices with FTO substrates is not uniform in both the positive bias and negative bias regions. The emergence of various defects, such as ionic and interstitial, in the active layers of CZS is what causes the apparent differences in positive and negative loop regions. To prevent excessive current flow through the device, which might irreversibly rupture the films, the current compliance is set at a maximum value of ± 10 mA. This guarantees the safety of the device. The symmetric loop area in both positive and negative bias regions can be observed from Fig. 5. This demonstrates the device's bi-stability under the given bias voltage. From the hysteresis curves, it can be seen that the devices possess good stability and endurance during the complete 100 cycles of operation. The dwell time is calculated by analyzing the time interval for completing the switching cycles. This refers to the amount of time that a memory cell or element retains its stored information before it needs to be refreshed or rewritten. The observed dwell time for 100 cycles is 62.1 s. During this period, the device is completely stable without any closing of the loop area. The device is initially in a low conducting state. The terms SET and RESET, respectively, are used to describe the positive and negative peak voltages.

An external bias voltage in the range of – 2 V to + 2 V was given to the fabricated devices. The observed loop regions lie between – 1.45 V and + 0.6 V. The pinched hysteresis loop in Fig. 5 can be explained with different stages of processes in which the loop occurs at different bias conditions. At first stage (stage 1), the current has a constant value up to 0.3 V. A sharp increase in current value occurs after 0.3 V and reaches a point of approximately 10 mA at 0.6 V (stage 2). The stage 3 arises due to the pre-set value of current compliance at 10 mA, which is set for the safety of the device [20, 21]. After the cutoff stage (stage 3), the current traverse along a different path with decrease in applied voltage, indicated by stage 4. The stage 1–3 constitute the SET process of the devices. Furthermore, when the reverse voltage is applied the current decreases in proportion to the reverse voltage up to – 1.1 V (stage 5). After the cutoff at stage 6, current retraces and the loop finally get complete at stage 7. The writing operation is evident from the sudden increase in the current value (or RESET). An abrupt flow of high current occurs in the device with a positive peak voltage when the applied voltage is between + 0.6 V and – 1.45 V. In this case, the device is observed to be in a low resistance condition, or ON state. The Low Resistance State (LRS) state is

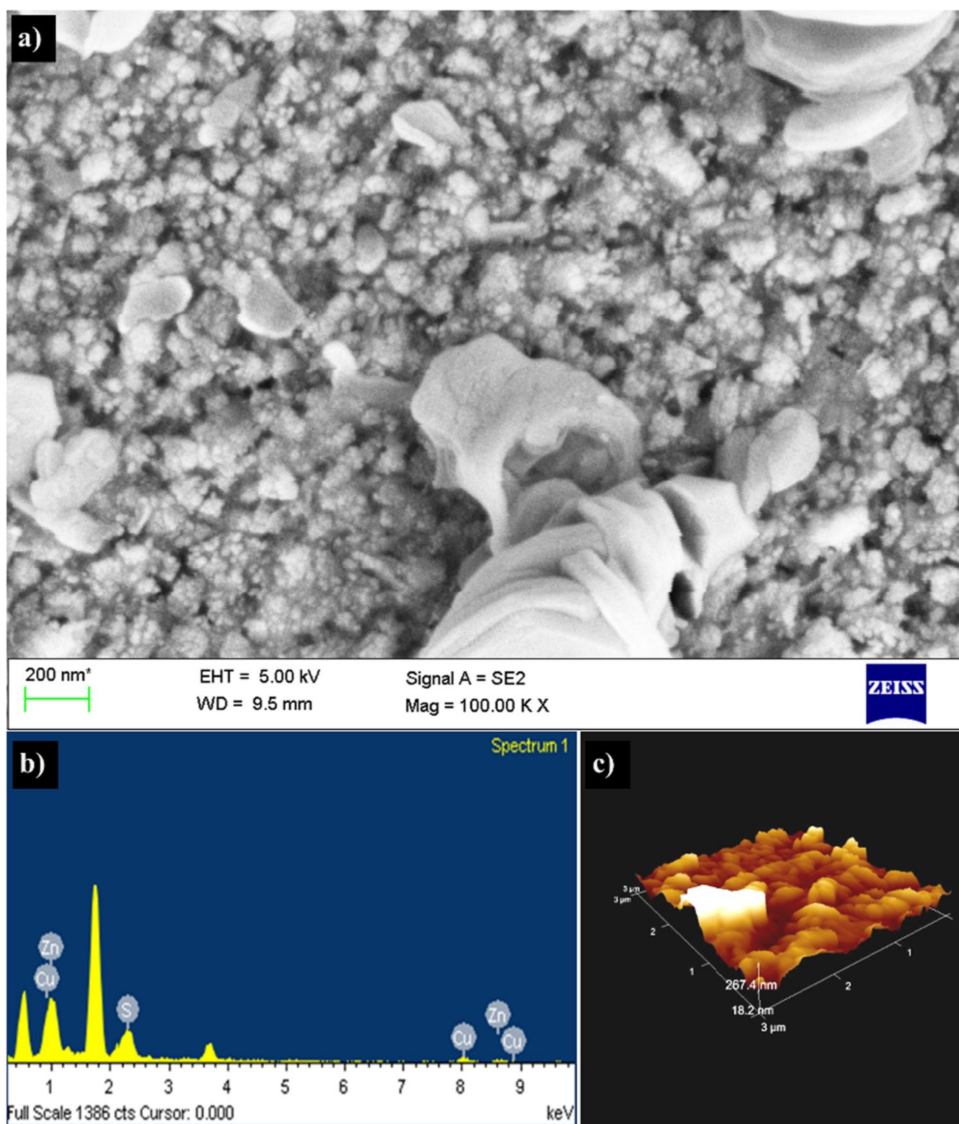

Fig. 3 **a** FESEM of the as-deposited CZS thin films at 350 ℃; **b** EDAX spectra of the distribution of elements; **c** AFM 3D topography of the CZS thin films deposited at 350 ℃

Table 1 Atomic percentage of constituent elements of as-deposited CZS film at 350 ℃

Element	Atomic%
S	39.09
Cu	32.33
Zn	28.59

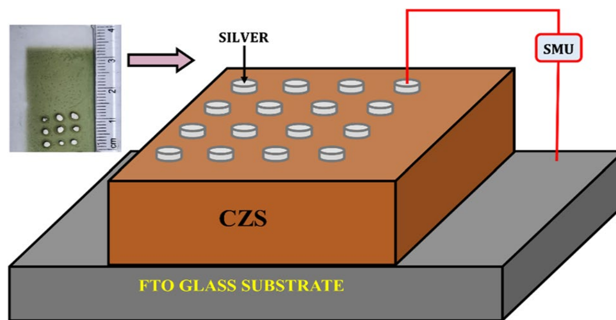

Fig. 4 Schematic diagram of FTO/CZS/Ag device and photograph of the device

prominent throughout the area that is extending from the origin. When the voltage changes from − 1.45 V to + 0.6 V, a small current with a negative peak voltage occurs in the circuit and in this particular state, the device is referred to be in the “OFF state” or “High Resistance State” (HRS).

The endurance characteristics of the FTO/CZS/Ag-resistive-switching device is shown in Fig. 6. For the fabricated

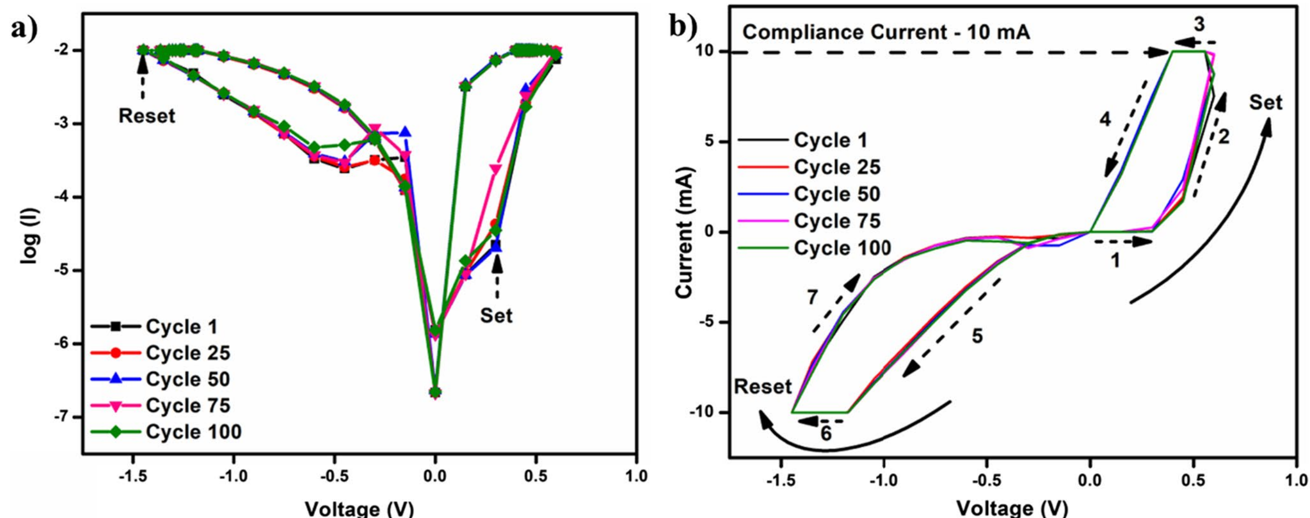

Fig. 5 **a** Log (I) – V characteristics of the device in positive and negative bias regions. **b** Pinched hysteresis current–voltage (I–V) loops of the FTO/CZS/Ag device

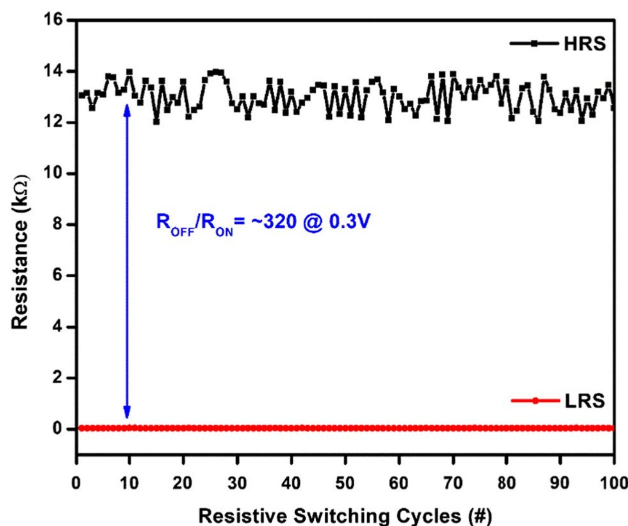

Fig. 6 Endurance characteristics of FTO/CZS/Ag-resistive-switching device

device, both cycles (SET–RESET and RESET–SET) have been repeated 100 times. Even after 100 cycles, the device's LRS and HRS exhibit good reproducibility and low fluctuations.

The average values of HRS and LRS are 13,020 kΩ and 40.65 Kω, respectively. For the FTO/CZS/Ag memory device, the calculated I_{ON}/I_{OFF} (R_{OFF}/R_{ON}) ratio is 320, which is the highest reported value for a device using CZS as the active layer.

There are three types of mechanisms proposed to understand the conduction processes of resistive memory-switching devices. ohmic conduction (OC), where the slope value of the fitted curve is roughly equal to unity, is called Type-I conduction. OC, also known as linear conduction, occurs when the resistance of the material itself primarily determines the resistance of the device, and the current–voltage (I–V) relationship follows Ohm's law (I α *V*). Trapped-charge-limited current (TCLC) and space charge limited current (SCLC) are Type-II and Type-III conduction, respectively [4, 5, 7]. Trapped-charge-limited current is a conduction mechanism that involves the movement of charge carriers (e.g., electrons or holes) through traps or defects in the device material. The current in this regime can be described using the Mott–Gurney law:

$$I = \varepsilon_0 \varepsilon A \mu {V^2}/{d^3} \tag{1}$$

where *I* is the current, ε is the dielectric constant of the material, ε_0 is the vacuum permittivity, *A* is the area of the device, μ is the mobility of the charge carriers, *V* is the applied voltage and d is the distance between the electrodes. Space-limited current, also known as Poole–Frenkel conduction, occurs when charge carriers hindered by an electric field within the material. This mechanism is often associated with high-voltage biasing, and it can be described by the Poole–Frenkel equation:

$$I = \alpha \varepsilon \varepsilon_0 A \exp\left(\frac{\beta v}{kT}\right)/d \tag{2}$$

where *I* is the current, α is a constant, ε is the dielectric constant of the material, ε_0 is the vacuum permittivity, *A* is the area of the device, β is a constant, *V* is the applied voltage, *k* is Boltzmann's constant, *T* is the absolute temperature and d is the distance between the electrodes.

The I–V curves are plotted in double logarithmic coordinates to assess by linear fitting to comprehend the conduction mechanisms of resistive-switching devices. The double logarithmic properties of the FTO/CZS/Ag device for both positive bias and negative bias are shown in Fig. 7a, b.

Figure 7a depicts the double logarithmic graph of the positive bias zone. Two major slopes observed during the LRS stage and only one during the HRS stage. From the graph, the slope value of 1.36 approximated to SCLC conduction mechanism ($I \alpha V^2$) and slope value of 4.89 contributes to the TCLC conduction mechanism. The slope value in the HRS state is 1.17. This value nearly comes under ohmic conduction mechanism ($I \alpha V$). In the negative bias region (Fig. 7b), two slopes corresponding to LRS region having values 3.58 and 3.77 are observed. This corresponds to TCLC conduction mechanism ($I \alpha V^n$, $n > 2$). In the HRS region, a single slope with value 1.87 obtained. The particular slope indicates nearly an SCLC conduction mechanism in which a special case happens when slope value nearly equal to 2, termed as the Child's law mechanism. Figure 8a–f denotes the curve fitting analysis of the positive and negative bias associating the conduction mechanisms present in FTO/CZS/Ag memory devices.

It is clear that the device constitutes different types of conduction mechanisms as observed from the calculations. From the studies reported in our earlier work, the band-gap, work function and electron affinity for the p-type CZS are 1.84 eV, 4.58 eV and 4.4 eV, respectively [11]. This work function merges with Ag (4.35 eV) and FTO (4.4 eV) electrodes which allows the easy flow of carriers through the interface. Using contact measurement, the resistivity of FTO and Ag contacts measured and obtained as ~ 8 Ω/sq.cm and ~ 10 Ω/sq.cm, respectively. The ohmic nature of contacts were confirmed using I–V measurements. Figure 9 describes the band diagram showing the junction formation schematics of the FTO/CZS/Ag device. The band alignment of the junctions can be understood from the diagram.

The electrical conductivity can vary reversibly and last for a long time between a high conductive (ON) state and a high resistive (OFF) state if a bias voltage is supplied between the electrodes. Since the external electric field is in the opposite direction after applying a reverse voltage to the Ag metal contact, the depletion region narrows down. This reduces the inherent electric field of Ag/CZS junction, which gives rise to the low resistance state of the device. On the other hand, the internal electric field exhibits high resistance behavior and the depletion zone extends in the same direction as the external field. Cu^{2+} has greater mobility in CZS thin films [22]. A decrease in copper concentration occurs at the CZS/Ag contact if a positive bias voltage is given to the Ag metal contact, causing Cu^{2+} ions begin to drift towards the FTO contact.

The schematic diagram shown in Fig. 10 describes the continuous forming and breakage of the conductive filaments. The CZS/Ag junction's depletion area is in a high resistance condition during the SET process. From this point, the reverse voltage on Ag gradually increases as the Cu^{2+} ions drift towards the Ag electrode, progressively producing Cu filaments. Here, the transformation from HRS to LRS takes place. The depletion-region of the Ag/CZS contact widens when the forward bias voltage is applied to

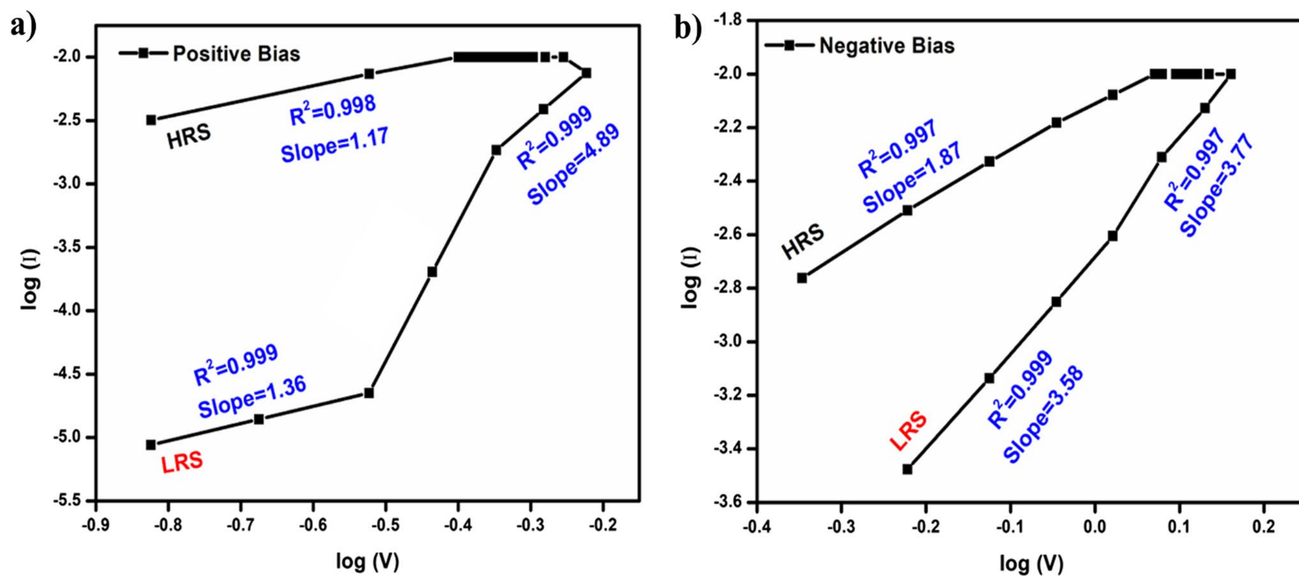

Fig. 7 **a**, **b** Double logarithmic characteristics of FTO/CZS/Ag device for positive/negative bias

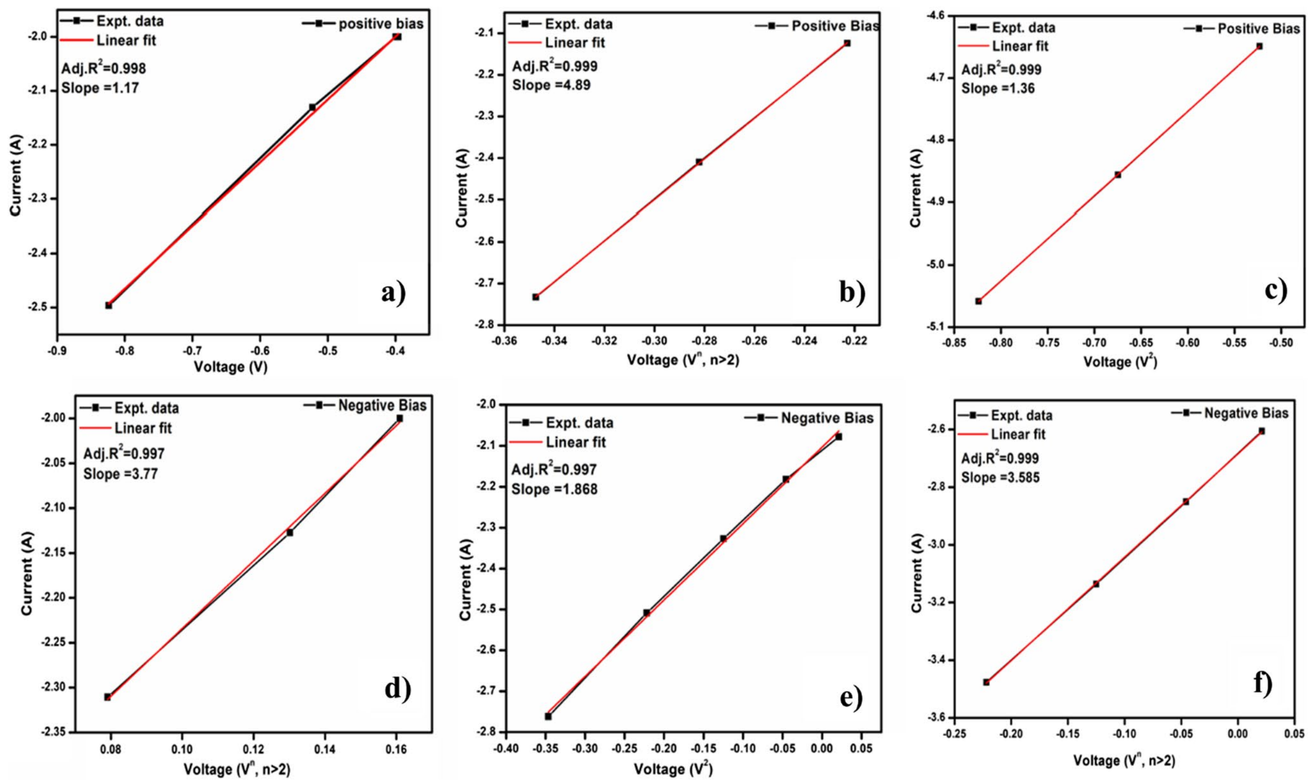

Fig. 8 **a–f** Fitted data of positive and negative bias showing various conduction mechanisms of FTO/CZS/Ag device

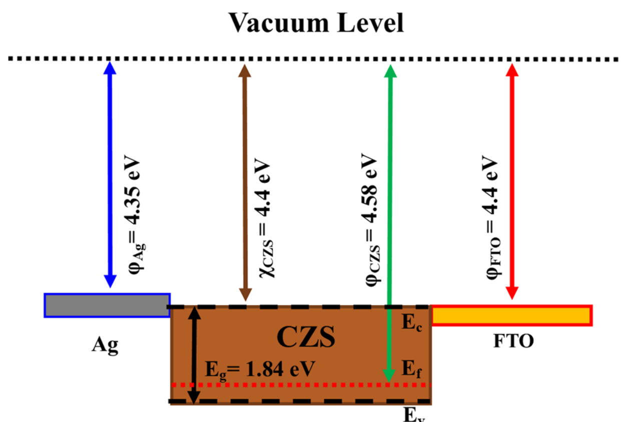

Fig. 9 Schematic energy band diagram of FTO/CZS/Ag device

the Ag contact, allowing Cu^{2+} ions to wander towards the FTO contact. When the forward voltage is raised further, the Cu conductive filaments rupture at a certain voltage as a result of Joule heating, and the device enters a RESET state. Finally, the conductive filaments begin to disappear, and conductivity is gradually replaced by the transmission of space charge. The filaments completely burst, and the device is still in HRS.

Table 2 compares the current result to the reported work on memory-switching devices. The table lists different deposition methods for producing memory-switching devices along with information on their endurance properties. Metal oxides such as NiO, TiO_2, ZnO, CuO, etc. are the most common materials used for the active layer in memory-switching devices. Many device structures are reported and wide range of active layer compounds are being tried to develop memory-switching devices that can perform fast switching properties and high endurance characteristics. Reported device architectures include single and double active layer structures. The present study achieved a higher $I_{ON/OFF}$ ratio of 320 using earth abundant material, which was deposited by a low cost technique of spray pyrolysis method. The ON/OFF ratio obtained is higher than majority of the reported values and comparable to metal-oxide-based memristors. Hence, it is evident that from the current investigation, CZS thin-film-based memristor devices have the potential to compete with widely used metal-oxide-based-switching devices. Further investigations are required to ascertain the retention time and the long term stability of the fabricated devices.

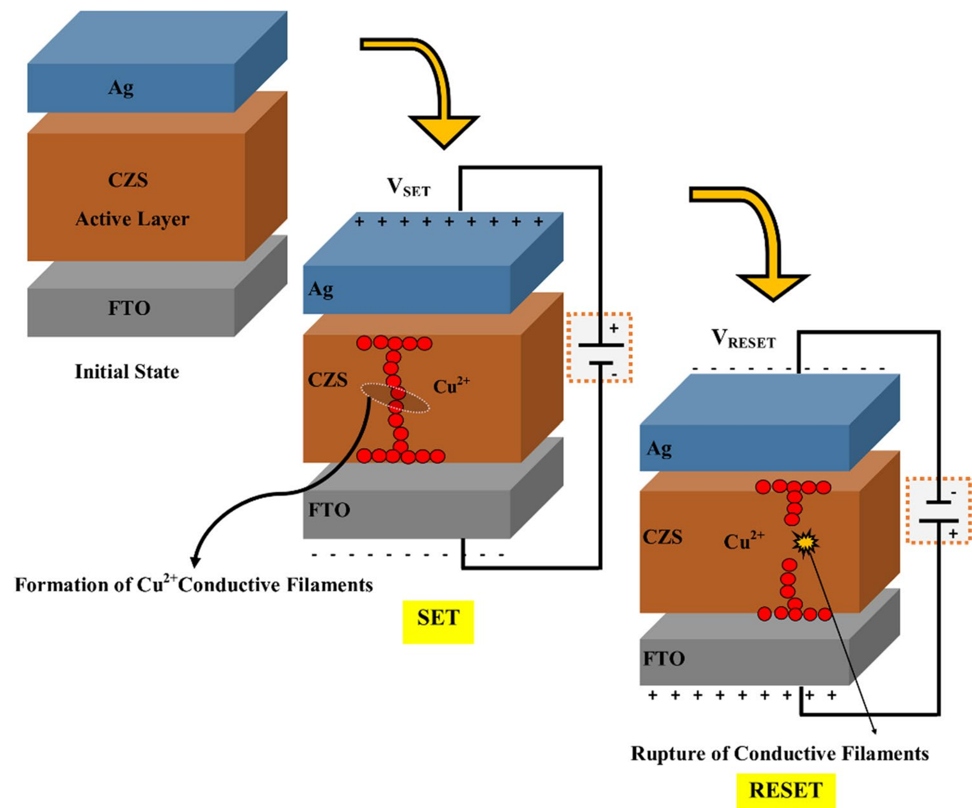

Fig. 10 Schematic diagram showing the formation and rupture of conductive filaments of FTO/CZS/Ag device

Table 2 Comparison of present study of the endurance characteristics with state of the art devices having metal oxide and chalcogenide compounds as active layer

S. No	Device structure	Fabrication technique	$i_{on/off}$ ratio	References
1	$Pt/Ta_2O_{5-x}/Ta$	RF sputtering	~ 10 and ~ 10^3	[23]
2	$Au/TiO_2/ZrO_2/FTO$	Dip/spin coating	100	[7]
3	Al/CZTSSe/Mo	Spin coating	27.5	[14]
4	Cu/CuO/(AgO)/Ag	Oxidation and printing	10	[24]
5	Pt/p-NiO/n-MgZnO/Pt	sol–gel spin-coating	6	[25]
6	Al/ZnO/Al	DC sputtering	2	[26]
7	$ITO/MoO_3/Ag$	Spray pyrolysis	1.2	[27]
8	FTO/CZTS/Ag	Spray pyrolysis	33	[13]
9	FTO/CZS/Ag	Spray pyrolysis	320	Present work

4 Conclusion

Using a low-cost spray pyrolysis process, CZS thin films were deposited and the electrical bi-stability of the memristor device FTO/CZS/Ag device was investigated. The changeover from a low conducting state to a high conducting state demonstrated the device's strong electrical bi-stability. With a high R_{OFF}/R_{ON} ratio of 320, the devices demonstrated good endurance capabilities. A model has been constructed to illustrate the memory-switching characteristics of the fabricated devices. From this investigation, it is shown that the fabricated devices FTO/CZS/Ag exhibit good electrical bi-stability under low bias voltage. This investigation opens up an opportunity for fabricating memory-switching devices with sulfide-based compounds.

Author contributions Conceptualization: MCSK, PA; methodology: MCSK, PA; formal analysis and investigation: PA, SSGS, RA; writing—original draft preparation: PA; supervision: MCSK.

Funding No funding received for this research work.

Data availability The authors declare that the data supporting the findings of this study are available within this paper.

Declarations

Conflict of interest The authors have no conflicts of interest to declare that are relevant to the content of this article.

References

1. B. Balraj, C. Sivakumar, P.F. Chung, M. Bharathi, S. Kumar Nagarajan, M.S. Ho, Mater. Lett. **308**, 131123 (2022)
2. T. Yanagida, K. Nagashima, K. Oka, M. Kanai, A. Klamchuen, B.H. Park, T. Kawai, Sci. Rep. **3**, 1 (2013)
3. A. Pradel, N. Frolet, M. Ramonda, A. Piarristeguy, M. Ribes, Phys. Status Solidi Appl. Mater. Sci. **208**, 2303 (2011)
4. P.K. Sarswat, Y.R. Smith, M.L. Free, M. Misra, ECS J. Solid State Sci. Technol. **4**, Q83 (2015)
5. N. Bitri, S. Mahjoubi, M. Abaab, I. Ly, Mater. Lett. **219**, 194 (2018)
6. K.H. Chen, T.M. Tsai, C.M. Cheng, S.J. Huang, K.C. Chang, S.P. Liang, T.F. Young, Materials (Basel). **11(1)**, 43 (2017)
7. H.C. Liu, X.G. Tang, Q.X. Liu, Y.P. Jiang, W.H. Li, X. Bin Guo, Z.H. Tang, Ceram. Int. **46**, 21196 (2020)
8. M.S. Sreejith, D.R. Deepu, C. Sudhakartha, K. Rajeevkumar, K.P. Vijayakumar, J. Renew. Sustain. Energy. **8**, 023502 (2016)
9. N. Kitagawa, S. Ito, D.-C. Nguyen, H. Nishino, Nat. Resour. **04**, 142 (2013)
10. E. Jose, M.C. Santhosh Kumar, J. Alloys Compd. **712**, 649 (2017)
11. P. Aabel, M.C. Santhosh Kumar, Int. J. Energy Res. **44**, 7778 (2020)
12. S. Bera, A.K. Katiyar, A.K. Sinha, S.P. Mondal, S.K. Ray, Mater. Des. **101**, 197 (2016)
13. P. Aabel, S. Sai Guru Srinivasan, R. Amiruddin, M.C. Santhosh Kumar, J. Mater. Sci. Mater. Electron. **34**, 1 (2023)
14. X.F. Dong, Y. Zhao, T.T. Zheng, X. Li, C.W. Wang, W.M. Li, Y. Shao, Y. Li, J. Phys. Chem. C **125**, 923 (2021)
15. S.P. Madhusudanan, K. Mohanta, S.K. Batabyal, J. Solid State Electrochem. **23**, 1307 (2019)
16. Z. Hu, F. Cao, T. Yan, L. Su, X. Fang, J. Mater. Chem. C. **11**, 244 (2022)
17. A.M. Diamond, L. Corbellini, K.R. Balasubramaniam, S. Chen, S. Wang, T.S. Matthews, L.W. Wang, R. Ramesh, J.W. Ager, Phys. Status Solidi Appl. Mater. Sci. **209**, 2101 (2012)
18. M. Adelifard, H. Eshghi, M.M. Bagheri Mohagheghi, Opt. Commun. **285**, 4400 (2012)
19. K. Yang, Y. Nakashima, M. Ichimura, J. Electrochem. Soc. **159**, H250 (2011)
20. S. Yu, X. Guan, H.S.P. Wong, Appl. Phys. Lett. **99**, 16 (2011)
21. H. Hu, A. Scholz, S.A. Singaraju, Y. Tang, G.C. Marques, J. Aghassi-Hagmann, Appl. Phys. Lett. **119**, 112103 (2021). https://doi.org/10.1063/5.0058526
22. N. Ciocchini, M. Laudato, M. Boniardi, E. Varesi, P. Fantini, A.L. Lacaita, D. Ielmini, Sci. Rep. **6**, 1 (2016)
23. A.R. Lee, Y.C. Bae, G.H. Baek, J.B. Chung, S.H. Lee, H.S. Im, J.P. Hong, J. Mater. Chem. C **4**, 823 (2015)
24. S. Zou, P. Xu, M.C. Hamilton, Electron. Lett. **49**, 829 (2013)
25. X. Chen, H. Zhou, G. Wu, D. Bao, Appl. Phys. A Mater. Sci. Process. **104**, 477 (2011)
26. F. Gul, H. Efeoglu, Superlattices Microstruct. **101**, 172 (2017)
27. A. Rasool, R. Amiruddin, S. Kossar, M.S. Kumar, J. Mater. Sci. Mater. Electron. **33**, 2090 (2022)

Publisher's Note Springer Nature remains neutral with regard to jurisdictional claims in published maps and institutional affiliations.

Springer Nature or its licensor (e.g. a society or other partner) holds exclusive rights to this article under a publishing agreement with the author(s) or other rightsholder(s); author self-archiving of the accepted manuscript version of this article is solely governed by the terms of such publishing agreement and applicable law.